

Optical Element Thermal Modeling for JWST to Support System Level Ground Tests

Randy Franck[1] and Russell B. Schweickart[1]
Ball Aerospace & Technologies Corp., Boulder, CO 80301
Sang Park[2]
Smithsonian Astrophysical Observatory, Cambridge, MA 02140
and
Dan Meagher[3]
ATK Space Systems Division, Houston, TX, 77058
and
Carl Reis[4]
NASA/Johnson Space Center, Houston, TX 77058
and
Wes Ousley[5]
Genesis Engineering Solutions, Inc., Lanham, MD 20706

The James Webb Space Telescope (JWST) observatory currently under construction is scheduled for launch in 2018. This telescope has a large aperture, and an infrared-optimized telescope passively cooled to below 50 Kelvin. As a part of the JWST test program, optical elements of telescope assembly will be exposed to the simulated operational environment within the newly renovated Chamber A at NASA Johnson Space Center. These optical elements will be cooled to their cryogenic operational temperature from normal ambient temperature. During the cool-down and warm-up transitions of each test, maximum allowable temperature gradients are imposed to minimize thermally induced stress that may potentially harm the hardware. This paper describes the evolution of the JWST optical element thermal models needed to predict these gradients during system level tests with the intent of minimizing test durations without exceeding allowable stresses during the temperature transition phases of the tests. These environments include helium cooled shrouds and the use of rarified gas to accelerate transitions. The thermal models have been matured using data from high vacuum as well as low-pressure helium gas environments during subsystem level testing. This paper also describes the system level thermal model of the test article developed from sub-system optical element thermal models. Applying chamber cool-down and warm-up profiles to this model will provide temperatures, temperature rates and chamber pressures to be used in system level testing based on allowable temperature gradient limits of the hardware under test.

[1] Principle Engineer, Cryogenics and Thermal Engineering Dept., 1600 Commerce St., Boulder, CO 80301/MS RA-6.
[2] Principle Engineer, Cryogenics and Thermal Engineering Dept., 1600 Commerce St., Boulder, CO 80301/MS CO-8.
[3] Engineer, Central Engineering, 100 Acorn Park Drive, Cambridge, MA 02140/MS05
[4] Thermal Analysis Engineer, Thermal Analysis and Electrical Design, 2224 Bay Area Blvd, Houston, TX, 77058.
[5] JWST OTIS Test Director, Energy and Space Simulation Group, 2101 NASA Pkwy, Houston, TX, 77058
[6] Senior Thermal Engineer, 4501 Boston Way, Lanham, MD, 20706

Nomenclature

ACF = Auto-Collimating Flat Mirror(s)
AOS = Aft Optics Subsystem
BATC = Ball Aerospace & Technologies Corp
CS = Center Section
CoCOA = Center of Curvature Optical Assembly
CTE = Coefficient of Thermal Expansion
FMC = Free Molecular Conduction
FMHT = Free Molecular Heat Transfer
GSE = Ground Support Equipment
GSFC = NASA Goddard Space Flight Center
HOSS = Hardpoint Offloader Support Structure
ISIM = Integrated Science Instrument Module
JSC = NASA Johnson Space Center
JWST = James Webb Space Telescope
K = Kelvin (unit of Temperature)
L2 = JWST Orbit: Second Lagrangian Libration point
L&C = Limitations and Constraints
mTorr = milli-Torr (unit of Pressure)
NASA = National Aeronautics and Space Administration
OGSE = Optical Ground Support Equipment
OTE = Optical Telescope Element
OTIS = OTE and ISIM Assembly
PF = PathFinder
PMSA = Primary Mirror Segment Assembly
SAO = Smithsonian Astrophysical Observatory
SINDA=Fluiint= Systems Improved Numerical Differencing Analyzer (C&R Technologies)
SINDA-G = Systems Improved Numerical Differencing Analyzer (MSC Software)
SMA = Secondary Mirror Assembly
SMM = Secondary Mirror Mount
TSS = Thermal Synthesizer System
UUT = Unit Under Test
XRCF = X-Ray Calibration Facility at NASA Marshall Space Flight Center

I. Introduction

The James Web Space Telescope (JWST) is a large space telescope that is to be launched later this decade. JWST is optimized to look at the universe in the infrared spectrum. In order to 'see' in the infrared wavelengths, the instruments suite and entire telescope have to reach deep cryogenic temperatures. Figure 1 shows the entire observatory. Everything above the tennis-court-sized deployable sunshield is at cryogenic temperatures. The major telescope optical elements are called out in the figure. JWST will enable scientists to investigate the origins of the cosmos and life in the universe. The L2 orbit, shielding of the sun/earth/moon system and passive, radiative heat rejection to space are the primary means JWST uses to reach operational cryogenic temperatures.

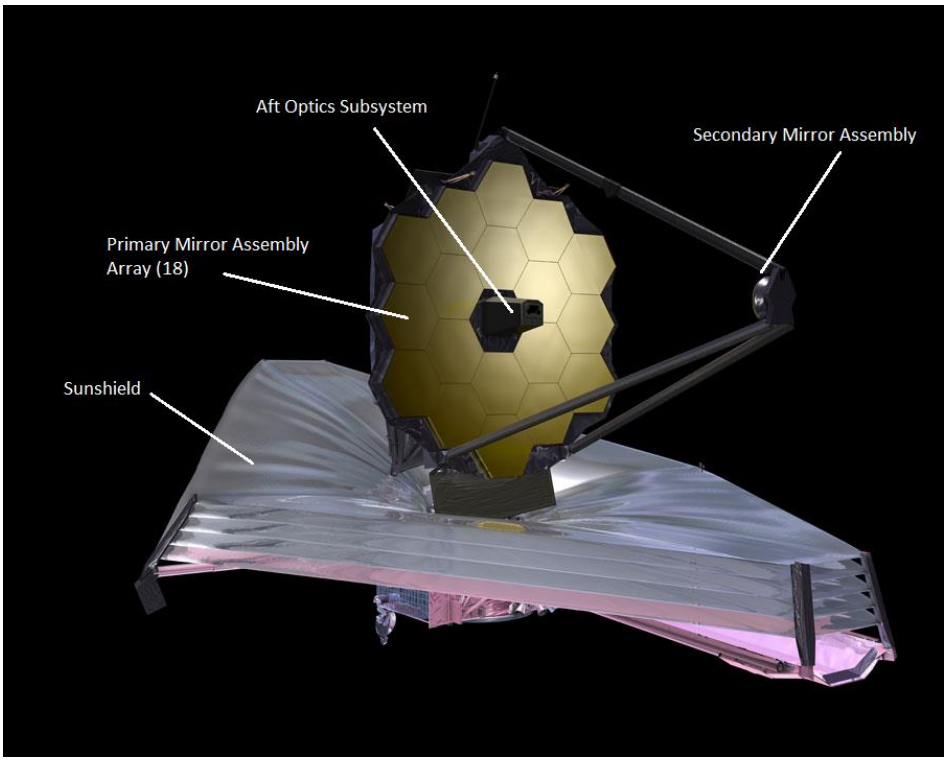

Figure 1. James Webb Space Telescope with Sunshield and Optical Elements Labeled.

Chamber A at Johnson Space Center (JSC), Figure 2, has been renovated to accommodate the JWST system level test campaign. These renovations include the installation of a helium shroud capable of <20K (in addition to the nitrogen shroud already in place), which is required in order for the Unit Under Test (UUT) to reach operational temperatures. Chamber A also now supports shroud operations with rarified gas to accelerate transition of the hardware. The chamber internal volume is sufficiently clean, both in particulates and molecular contaminants, to accommodate the highly sensitive JWST optical element assemblies. Furthermore, this chamber will also provide a low vibration environment conducive to making extremely precise optical measurements.

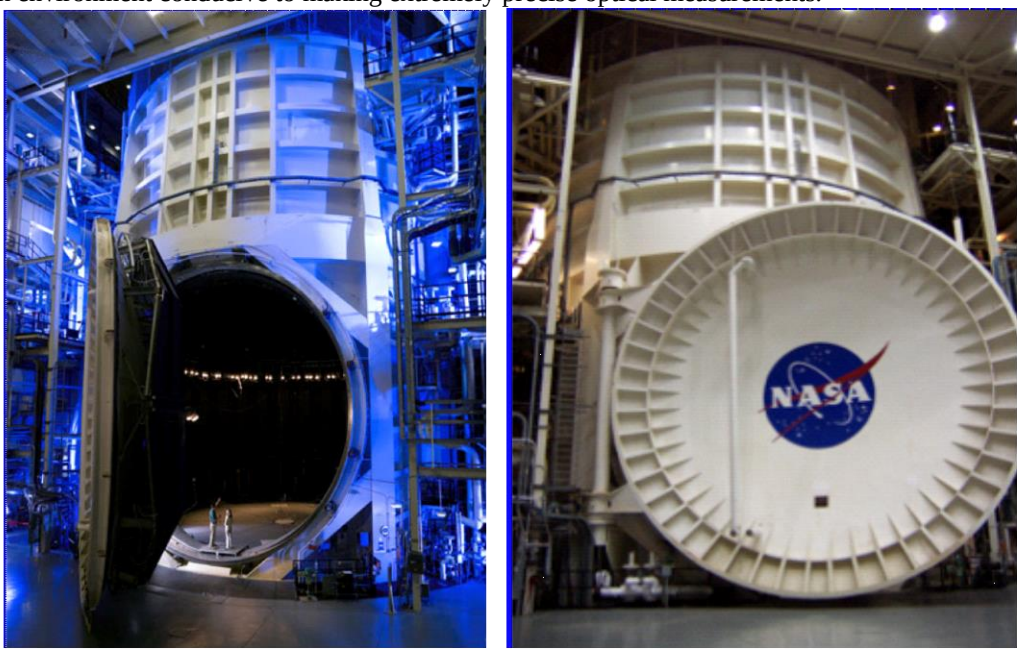

Figure 2. NASA JSC Chamber A with the chamber door open and closed respectively. Note the size of the chamber door (40 feet opening) with the persons standing in the left figure.

The JWST optical system will be cryogenically tested to verify optical performance at predicted temperatures. After the Integrated Science Instrument Module (ISIM) is integrated with the Optical Telescope Element (OTE), this combined assembly is called the OTIS. At the Chamber A thermal vacuum facility, the OTIS will undergo end-to-end optical and thermal tests at flight temperature levels (planned for 2017), with the JWST launch schedule depending on timely test completion. To reduce this schedule risk, a series of three tests will be executed in Chamber A prior to OTIS, using "pathfinder" hardware. In general, the "pathfinder" tests will check out the extremely complicated optical test hardware, chamber systems, team communications, procedures, and analyses. Test personnel will demonstrate the planned alignment and optical test processes, enable improvements in OTIS test efficiency and accuracy, and foster team-building and training in the test environment without significant risk to flight schedules or hardware. Useful information will also be generated on test hardware dynamic behavior and thermal performance, with particular emphasis on cooldown and warmup characteristics and techniques. The first test in the series is the Optical Ground Support Equipment test 1, or OGSE1

During ground tests, the large thermal mass of the UUT and the reliance of the flight design on passive cooling combine to cause the cool-down and warm-up portions of the test, or "cryotransitions," to dominate the schedule. This drives up the substantial 'marching army' costs and takes away valuable time from performance verification of the system at operational temperatures. In order to minimize cryotransition durations, a number of strategies will be employed. These include the large capacity helium shroud system for heat loads encountered while transitioning, use of rarified gas to create an efficient heat transfer mode in the cryogenic region, actively cooled Ground Support Equipment (GSE), and heaters on the flight hardware to manage cryotransition.

The OGSE1 is primarily an optical test, with the checkout of the OTIS optical test equipment as the main objective. The chamber systems, shrouds, and OGSE will be operated as a system during the Chamber Commissioning test several months prior, but OGSE1 will be the first time the OGSE can take nanometer-scale measurements of primary mirror segments in a configuration similar to the OTIS test. During OGSE1, some of the processes to be used for aligning and testing the OTIS will be thoroughly checked out, allowing test operators to verify test effectiveness and identify opportunities to improve accuracy and/or reduce test time. Other objectives include testing of primary mirror operations, dry runs of chamber installation procedures, and demonstration of systems for data, communications, and contamination control monitoring.

This test also directly helps prepare for the OGSE2 test scheduled several months after OGSE1. Since the flight Aft Optics Subsystem (AOS) will be installed for OGSE2, cryo load testing of the Pathfinder structure in OGSE1 is an important test objective. Also, the AOS must be quickly returned to the time-critical JWST integration flow, so the OGSE2 test timeline must be firmly established. Data developed from the OGSE1 gaseous-helium-assisted cooldown and warmup will contribute significantly to OGSE2 timeline estimation.

Limitations and Constraints (L&C's) have been established to ensure the safety of the hardware through cryotransition. Note that 'warm-up' from cryogenic temperatures to room temperature for JWST is not something that will happen in flight and is therefore specific to ground testing. To the extent possible, the L&C's will be monitored real time during cryotransition. However, it won't be possible to instrument and actively monitor all of the locations with L&C's during integrated system level testing. Therefore, the safety of the hardware will be reliant on the more sparse data that is available and extrapolation of that data to the areas lacking real time telemetry. In turn, hardware safety will be reliant on the ability to model and predict cryotransition, and to use those models to establish safe rates of change, gradients, and extrapolating between telemetry points. To this end, a number of completed subsystem tests that used cryotransition in rarified gas are being leveraged to correlate optical element thermal models to measured data.

II. System Test Configuration

The OGSE1 test article configuration is shown in Figure 3. The Pathfinder structure is similar to the flight JWST telescope backplane structure center section (CS), and is used to support the two primary mirror assemblies (PMSAs) and the secondary mirror (SMA). Because the Pathfinder structure was built years before the final structure design was completed, it is not identical to the flight structure. One of the PMSAs used in the OGSE1 and OGSE2 tests is a flight spare unit; the other PMSA and the SMA are engineering units.

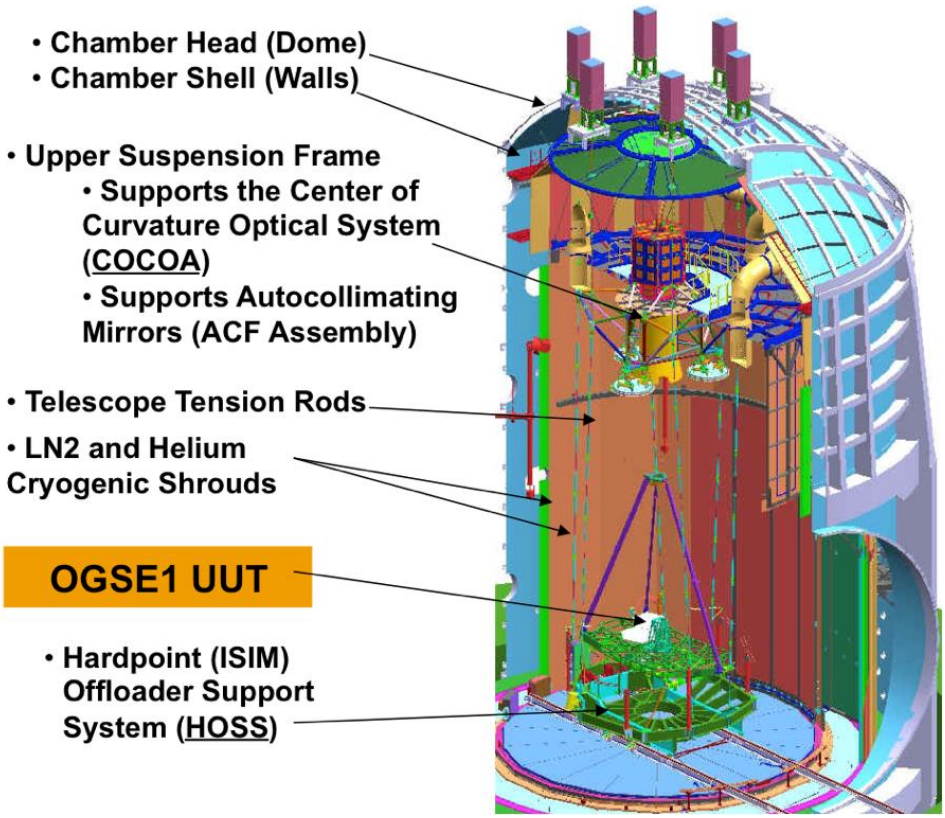

Figure 3. Sectional view of the OGSE1 test configuration with the UUT, including 2x PMSA's, with the JSC Chamber A features and optical-GSE components shown[1].

III. Schedule and Hardware Safety Considerations and The Need for Modified Thermal Models

Early estimates of the overall cryotransition schedule, with schedule allocation for hardware verification showed a reduction of 50 days when using rarified gas. The acceleration achieved with the rarified gas occurs primarily at colder temperatures. Radiation heat transfer tails off from its maximum at the beginning of cool-down when the shroud is cold and UUT is close to room temperature. The opposite occurs during warm up, with the rarified gas effect dominating until the shroud temperature can be safely raised to a level that radiation dominates heat flow from the UUT. In addition to the hardware safety considerations mentioned above, contamination control, including flight decontamination heater operations, and the risk of corona arcing due to Paschen effect in the rarified gas region can affect the duration of cryotransition.

Traditionally, the early focus of space-borne-program thermal analysis is operational performance in the flight environment. As hardware evolves, the model evolves to address specialized scenarios, such as contingency operations and ground test modeling. When cryotransition to support ground test campaigns is modeled, it is typically focused on duration, or overall schedule allocations. The historical modeling of JWST has supported these types of predictions. With sufficient instrumentation, L&C's can be monitored to protect the hardware. As the program moves into tests of higher levels of assembly, including the final test before flight however, this level of access and monitoring is not possible. Modified models able to more accurately predict intra-hardware gradients and rates in vacuum and rarified gas are required. Thermal model correlation of JWST is a challenge, even for quiescent, steady state thermal balance conditions at high-vacuum due to the telescope size and complexity of passive cooling. The additional challenge for ground-test cryotransition modeling is that we are looking for high accuracy, while predicting transient behavior on a dimensional scale rarely seen in our industry, and with the extra 'knob' of rarified gas altering the heat transfer dynamics.

Figure 4 compares an early prediction of the cooldown at the Marshall's X-Ray Calibration Facility (XRCF) where cryofiguring and verification of the Primary Mirror Segments (PMSA's) was performed. Pressure of the He

gas is plotted on the secondary Y-axis for reference. Note that the overall duration of the cooldown is well predicted (dashed line), but that the temperature of the mirror during bulk of the cooldown is not accurate. This chart illustrates the need to improve the accuracy of cryotransition thermal modeling.

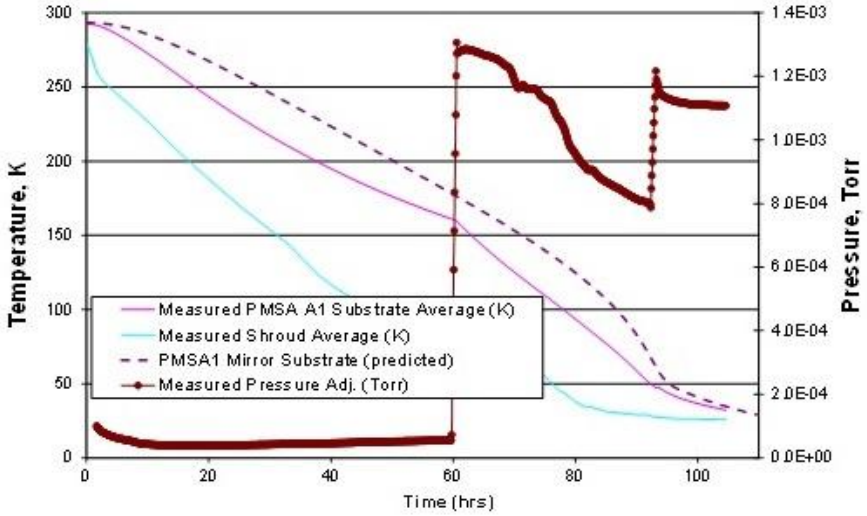

Figure 4. Comparison of Original Predictions of PMSA Cooldown to Measured Test Data.

Temperature gradient limits between different components of the PMSA have been established to protect the hardware. These limits are shown in Figure 5. Note that the gradient can produce either a negative or positive value depending on cooldown or warm up, the same absolute values apply. In this figure, negative values are shown. The allowable gradients are a function of temperature, with the allowable absolute gradient value increasing as the temperature decreases. This is a result of the decreasing Coefficient of Thermal Expansion (CTE) of the telescope structure and optical element materials as the hardware assembly cools, which in turn makes the strain induced by a gradient more benign at colder temperatures. L&C's such as these should be adequately conservative, but not so conservative that they could unnecessarily constrain the speed at which the hardware temperatures can change. Such L&C's should also be derived based on the temperature of major hardware elements. This increases the possibility that temperature sensors are already available, or can be added for ground tests to evaluate L&C's. Finally, basing the L&C on larger elements reduces the uncertainty in analytically predicting and extrapolating temperatures if sensors can't be used.

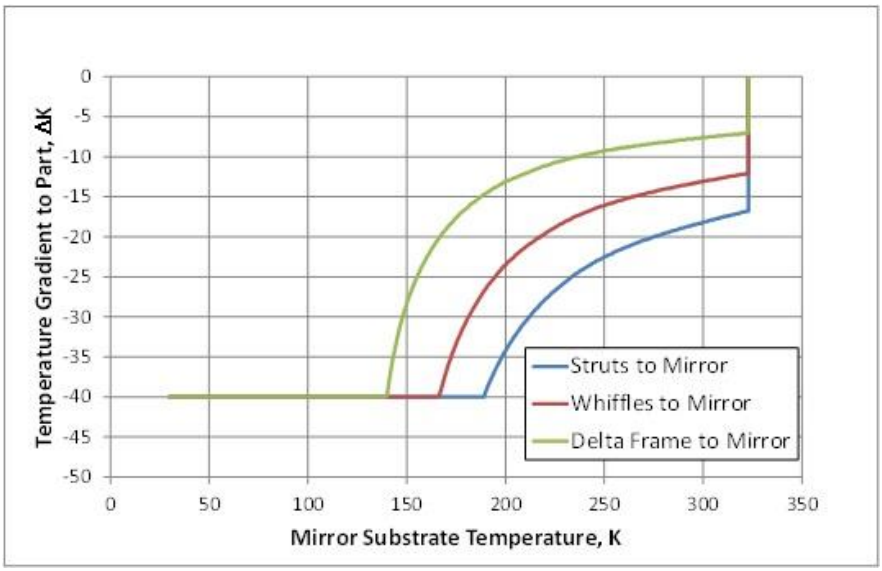

Figure 5. PMSA Cryotransition Limitations and Constraints.

Figure 6 shows the hardware components of the PMSA involved in the L&C's. Note that attaching sensors to these elements was relatively easy for subsystem level tests, unlike later tests at the OTIS level where access will be limited.

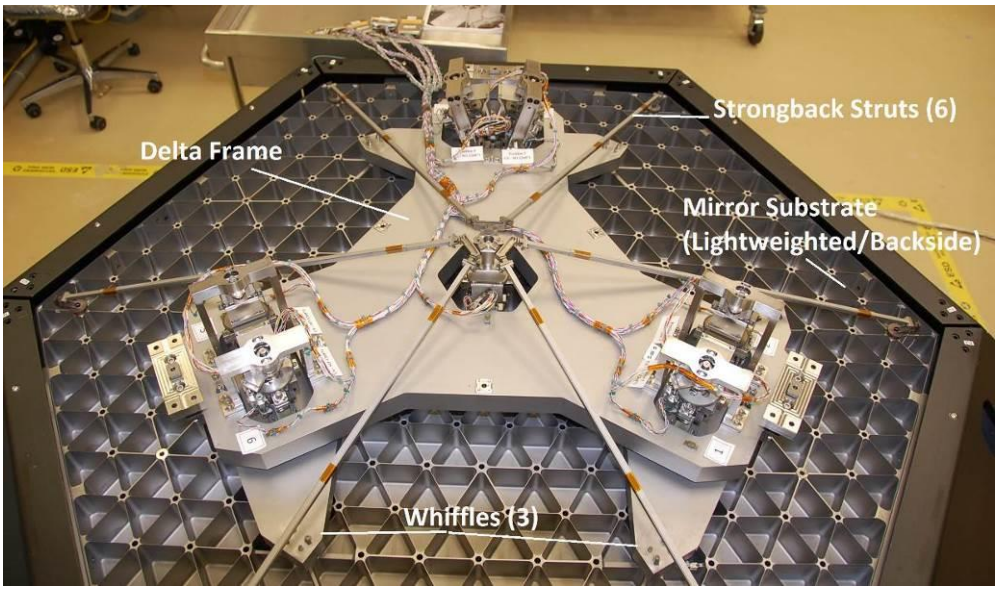

Figure 6. PMSA Construction Details (Black cover around perimeter is non-flight).

IV. Correlated Subassembly Model Development

Three OTE subassemblies are being correlated to cryotransition test data. The PMSA has been mentioned and is the first effort. The Aft Optics Subsystem (AOS) will follow, which houses both the tertiary mirror and the Fine Steering Mirror (FSM). Last will be the Secondary Mirror Assembly (SMA). The AOS and SMA were tested in a Ball Aerospace and Technology Corporation (BATC) vacuum chamber. The correlation effort for the test thermal models begins with modifying the flight thermal model. The flight models have served for on-orbit predictions well for years with modest changes and were generated in TSS and Sinda G. The sparse geometrical representation has been sufficiently accurate for the stable, low radiation heat exchange conditions of cryogenic flight operational predictions, while not overburdening the analysis computational time. Figure 7 shows the current geometry model for flight predictions.

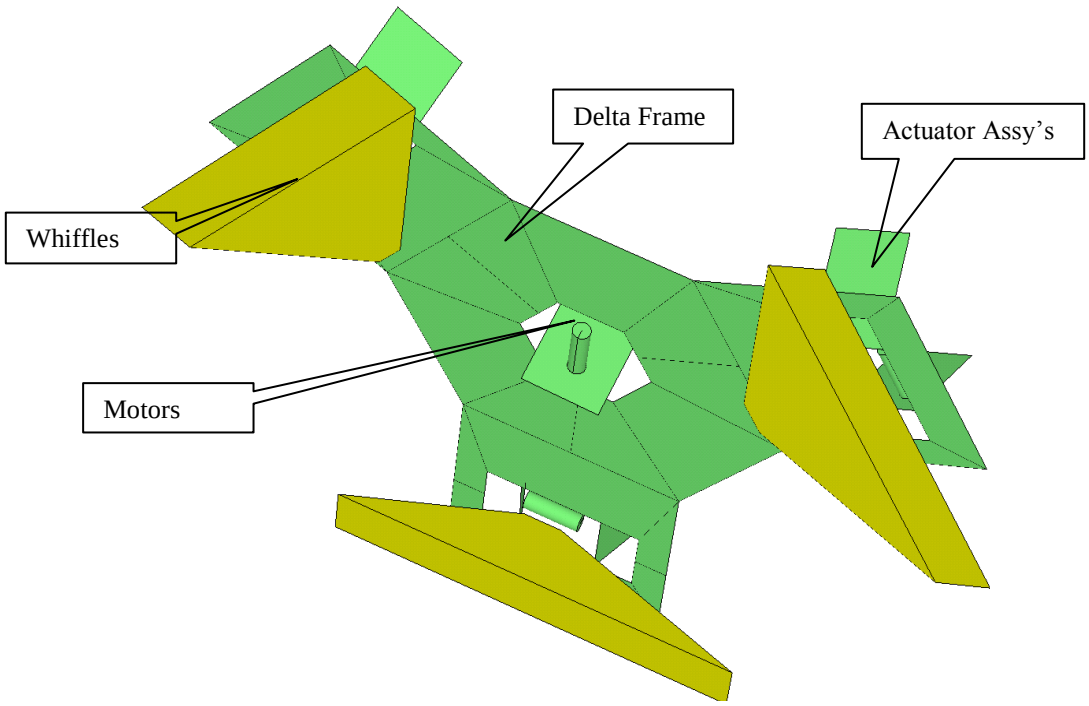

Figure 7. Current Flight PMSA Geometry Thermal Model Representation (Mirror substrate not shown).

A number of initial changes have been made to the heritage flight models to support cryotransition predictions:

- Conversion to Thermal Desktop® software consistent with the test thermal modeling campaign
- Added resolution of geometry to support the higher radiative heat exchange environment of cryotransition
- Added resolution of geometry to support rarified gas heat transfer
- Increased nodal resolution of the mirrors
- Inclusion of elements representing the strongback struts

The PMSA/XRCF correlation process will be divided into two regions; the higher temperature, high vacuum region at the onset of cooldown and end of warm up, and the lower temperature, rarified gas region at the end of cooldown and beginning of warm up.

Some of the available parameters for correlation span both regions. They include an accounting of material properties affecting transition. These are mass, specific heat, conductivity, and emissivity. While these properties have been evaluated in great detail over the course of the program, emphasis is often given to flight conditions. For example, the accuracy of specific heat and conductivity over the entire cryotransition temperature region must be included. Additionally, models that incorporate 'predicted mass with allocations', may be appropriate for models delivered prior to build, must be re-considered for accurate cryotransition analysis, especially if measured masses are available. Additionally, consideration is given to masses not resolved, or not resolved well in the flight models. Examples of this are harness sections that reside on large components. How does one represent this thermal transient effect without over-nodalizing the thermal model?

Harnesses attached to components highlights another challenge; how does one represent the emissivity of a complex assembly level surface, when it is represented with a simple surfaces and limited nodes in the thermal model? This is illustrated by the CAD image in Figure 8 of the back of the AOS FSM baseplate. Not only are there a multitude of light weighting features, but harness routing and bolted interfaces further remove the actual hardware emissivity from the simple geometry and uniform thermo-optical properties used in the model. Therefore, effective emissivities are used to account for this, and keep the model fidelity from becoming intractable. Due to the wide range of temperatures in the shroud volume during the cryotransition, grey body assumptions need to be challenged as well. For instance, during cooldown for grey body assumptions, the shroud emissivity/absorptivity should be based on the warmer UUT and GSE that are emitting to it, and not on the temperature of the shroud itself.

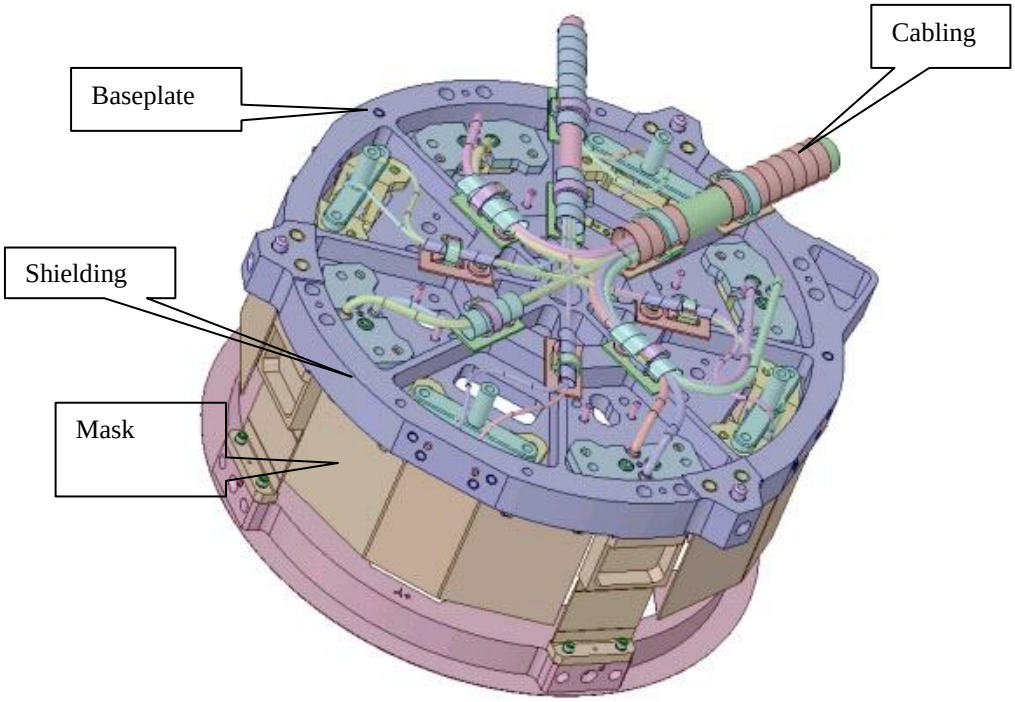

Figure 8. CAD Image of AOS FSM Baseplate as Viewed from Behind (mirror not shown) Illustrating the Complexity of the As-Built Thermal Capacitance and Emissivity Properties.

V. Case Study: PMSA's at XRCF

Figure 9 shows the Cryotest configuration of the PMSA's at XRCF as the UUT is being moved into the chamber. Measured data is used from this test to correlate the models. The facilities are treated as boundary conditions, and measured data is applied to the various components to drive them exactly as they did in test.

Figure 9. PMSA's at XRCF for Testing.

A. XRCF Test Models

The last three XRCF tests included 6 sets of flight PSMA assemblies, and each test subjected the mirror assembles to 2 thermal cycles down to 40 K. The final test (Test 8) has been used for model correlation. Figure 10 shows the PSMA segments present in this test. Figure 11 shows the mounting locations of test sensors in the XRCF chamber. Measurements from these sensors were averaged in 9 separate zones to represent transient boundary conditions in the thermal model. Since additional sensors were used to monitor the non-flight PMSA support rings and the support structure, these GSE components were also modeled as transient boundary conditions. The LN2 forward extension was assumed at 80K for the entire test duration along with the 293 K chamber window.

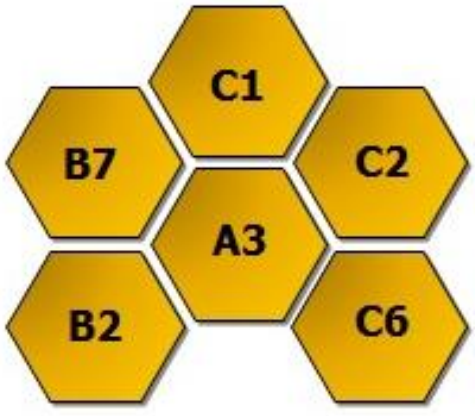

Figure 10. Segment Designation for XRCF Test 8.

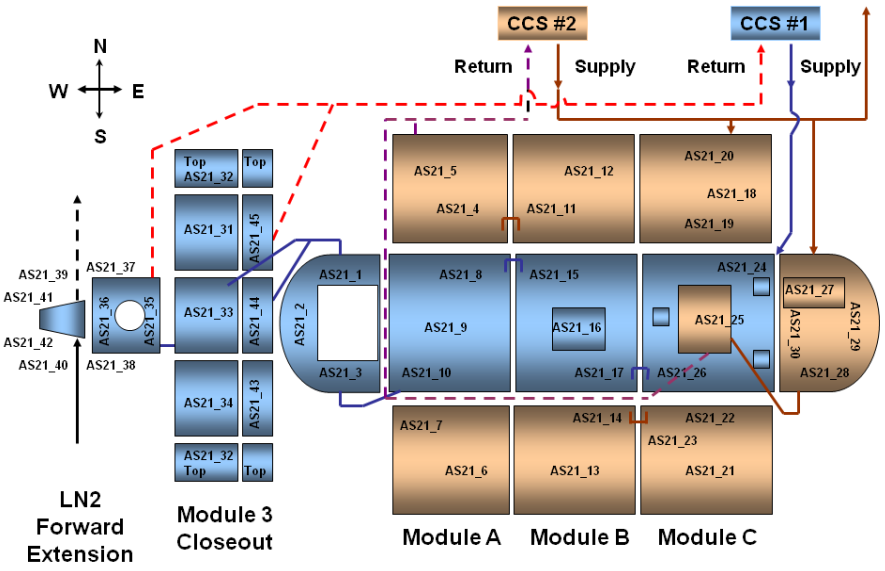

Figure 11. XRCF Chamber Sensor Locations and Cooling System Schematic.

B. PMSA Model

Shown in Figure 12 is the geometry used to represent the PMSA in the XRCF model. Actuator motors are modeled individually as well as the actuator support brackets, but all other actuator components were simulated with rectangular boxes. Changes from the flight geometric model to more accurately account for radiative heat transfer at warmer temperatures include adding the actuator support brackets, correcting locations of the motors, changing the representation of the actuator components, adding a third dimension to the delta frame, whiffles and mirrors, including the strongbacks and increasing the fidelity of the mirrors from one to 32 nodes. The model was developed in Thermal Desktop®, but other than for the strongbacks and mirrors, retains all node numbers and conductors associated with the original correlated SINDA-G PMSA model. Submodels were added for each mirror assembly to ease model integration and transfer. Node and conductor blocks from the original model were inserted into Node and Conductor Data blocks within Thermal Desktop® submodels as opposed to inserting them as a stand-alone "include" file. A comparison of steady-state flight heat flows from the updated model and the original SINDA-G model verified the translation with differences of less than 10 μW.

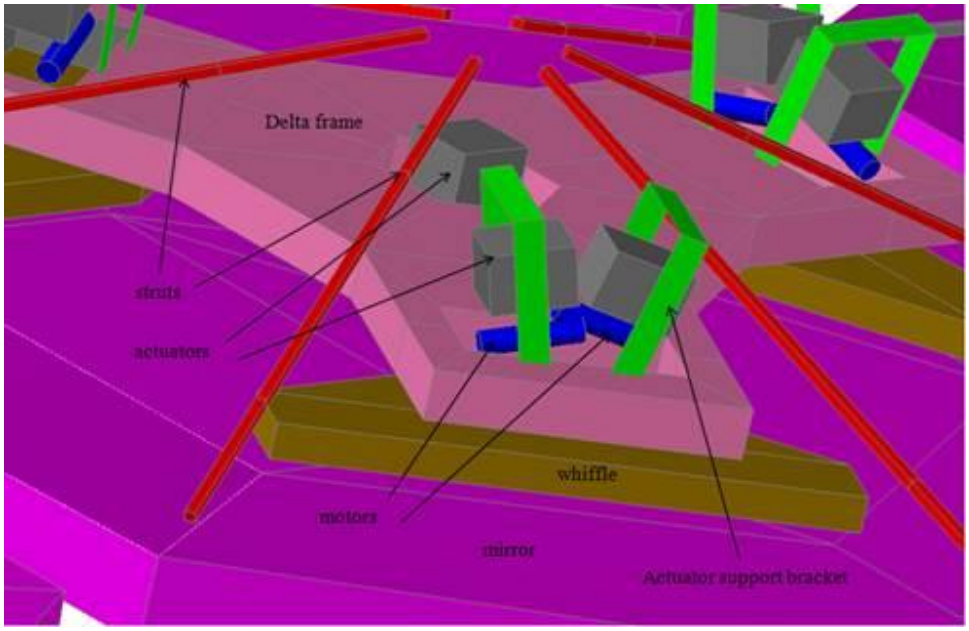

Figure 12. Updated Geometrical Representation of PMSA components in Thermal Model.

C. Cool Down Model Simulation

A cool down simulation involves dividing the cryo-transition into two periods: one at the start of the cool down when the chamber was at a high vacuum and heat transfer from the mirror assemblies to the chamber was predominantly radiative. The second applies after helium had been introduced into the chamber.

1. Analysis Prior to Helium

During the XRCF tests, helium was introduced into the chamber after the mirror temperatures had decreased to about 200 K, thus any heat transfer algorithms simulating rarified gas conduction could be omitted from the simulation of this phase of the test. For this reason, the start of the test should have been easier to correlate; however, analysis results showed the mirrors in the test cooled faster than expected at the start of the test and slower than expected toward the time (after about 32 hours) when helium was injected into the chamber. A comprehensive review of test model assumptions and the test configuration, including shroud emissivity, sensor bias, and possible heat sources failed to reveal a specific cause. Thus, the best candidate parameter to use to match the test data, since it contains the greatest modeling uncertainty, is the effective emissivity of the surfaces representing the back of the mirrors.

Due to the significant amount of computational time that would be required to simulate the radiative heat transfer between the surfaces associated with the complex geometry of the back of the mirrors, Shaun Thomson of NASA GSFC developed a set of data[2], shown in Figure 4, representing an effective emissivity of the back of the mirrors as a function of temperature if the mirror back were a flat surface. Without a specific test to verify this data, this approximation clearly represents a major uncertainty in the analysis results. For this reason, the effective emissivity of the back of the mirror was used in the model to correlate the analysis to the test results. However, the degree to which this function had to be changed from Thomson's recommendations for the model to match the test results seemed unreasonable. In Thomson's function, the mirror back emissivity only decreases to 0.42 from 0.48 between 300 and 200K. To match the test results, this value had to decrease to 0.15 at 200 K. A plot of the mirror back effective emissivity used in the model to correlate to test data is also shown in Figure 13.

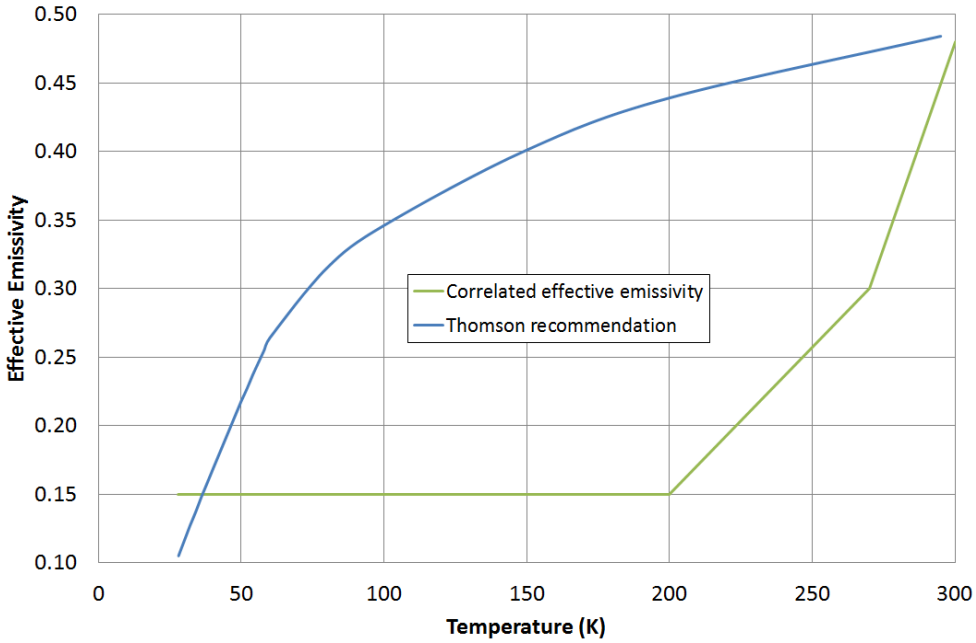

Figure 13. Effective Emissivity of Back of Primary Mirrors, Recommended by Thomson and Correlated.

Figure 14 shows how well the model results match the test data for two of the mirror segments with the correlated effective emissivity. While this effective emissivity dependence may seem unreasonable, it is necessary since one of the primary requirements of the correlated early-phase test model is that the temperatures match test results so that the late-phase test model starts with good initial conditions.

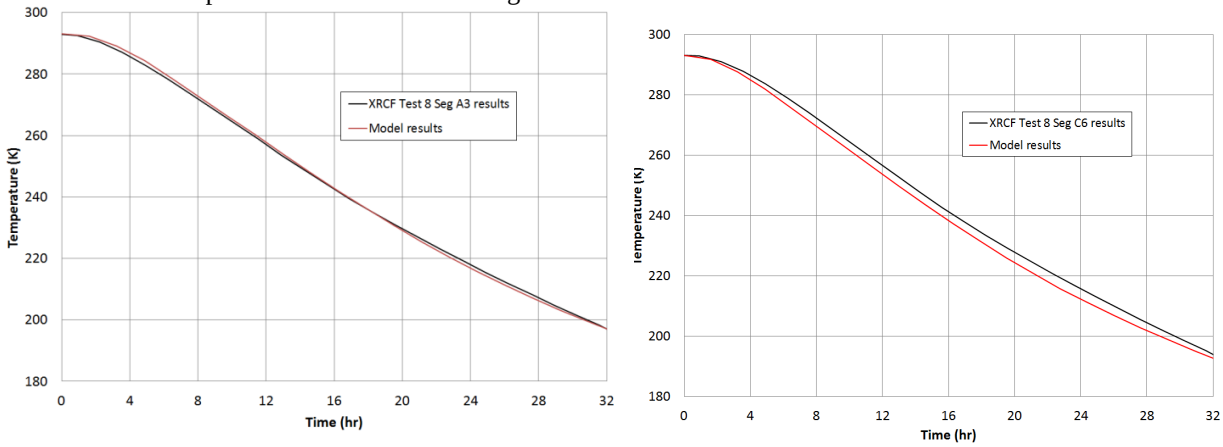

Figure 14. Measured and Correlated Temperatures for Two of the Mirror Segments During XRCF Test 8 Initial Cooldown.

Figure 15 shows model results for sensors on the whiffle, delta frame and one strut of mirror segment A3 (center mirror) during the same Test 8 cool down respectively. Since the struts are thermally isolated from the rest of the structure other than at the ends, correlation to test data is straight-forward; analytic results match that of the test best when the emissivity of the strut was assumed a fixed value of 0.18, which is a reasonable value for a featured beryllium metal finish.

The whiffle structures and delta frames have light-weighting pockets like the mirrors but the pockets are larger. Thus, their geometry is less complex, but for the same reason as the mirror backs, their effective emissivity, similarly modeled as flat surfaces, represents a modeling uncertainty. In the model, all surfaces of the whiffles and delta frames were assumed to have an emissivity of polished beryllium measured at room temperature at 0.111.

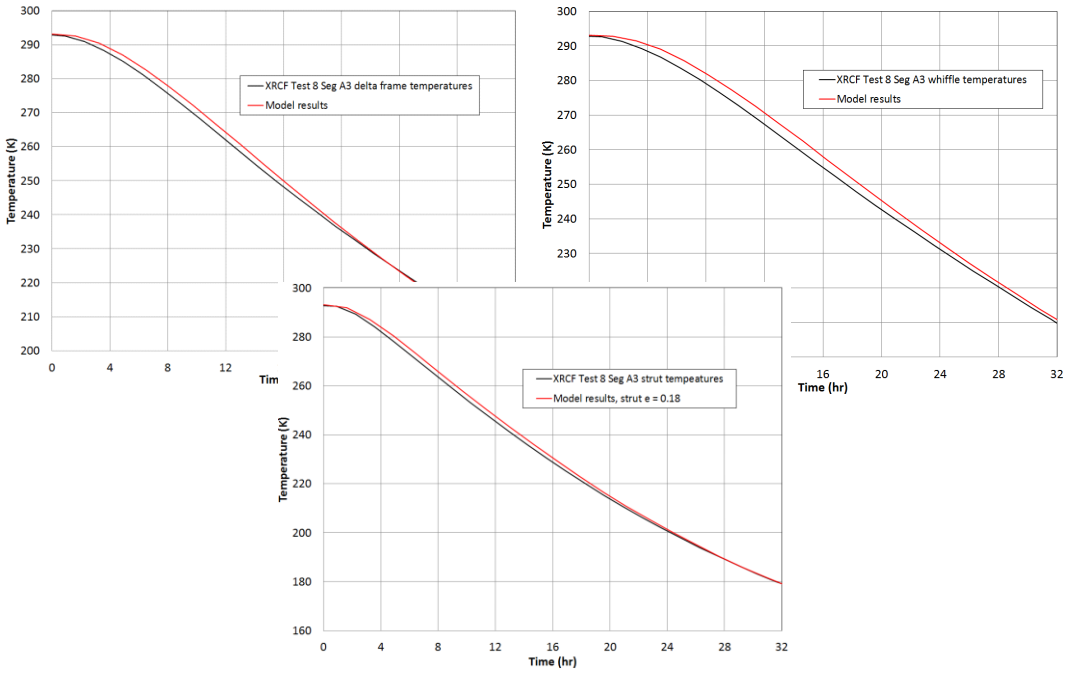

Figure 15. Measured and Correlated Temperatures for Delta Frame Whiffle and Strut of Segment A3 During XRCF Test 8 First Cool Down.

2. Accounting for Rarified Helium Gas Heat Transfer

Attempts were made to correlate the thermal model with test data using various methods of simulating rarified gas conduction. Only methods that could be incorporated into the models and associated solution routings without increasing simulation times excessively have been considered. For instance, a computational fluid dynamics (CFD) model was not considered. Methods considered include free molecular heat transfer and continuum gas conduction.

3. Free Molecular Heat Transfer

SINDA/FLUINT allows for a user-defined linear heat transfer conductor between surfaces based on the same view factors needed to compute heat transfer due to radiation. The primary intention of this conductor is to simulate free molecular gas heat transfer (FMHT). FMHT occurs when gas molecules transfer energy between surfaces without interacting with other gas molecules. If there are more than 100 collisions with other molecules between the two surfaces, the gas is considered a continuum. The mode of heat transfer is characterized by the Knudsen number, which is the ratio of the mean free path to characteristic length. Thus, if the Knudsen number is less than 0.01, the gas is in continuum; if greater than 1, the gas is in the free molecular region. Between these, the gas is in a transition region, which is more difficult to simulate. If the characteristic length can be defined as,

$$Lc = 4*V/A$$

where V is the chamber volume and A is the associated surface area, then the mode of heat transfer in the XRCF test should be primarily continuum as shown in Figure 7. So strictly speaking, free molecular heat transfer should not apply. Five of the mirrors are located near the chamber wall, however, so FMHT may be more appropriate for test components located near the chamber wall.

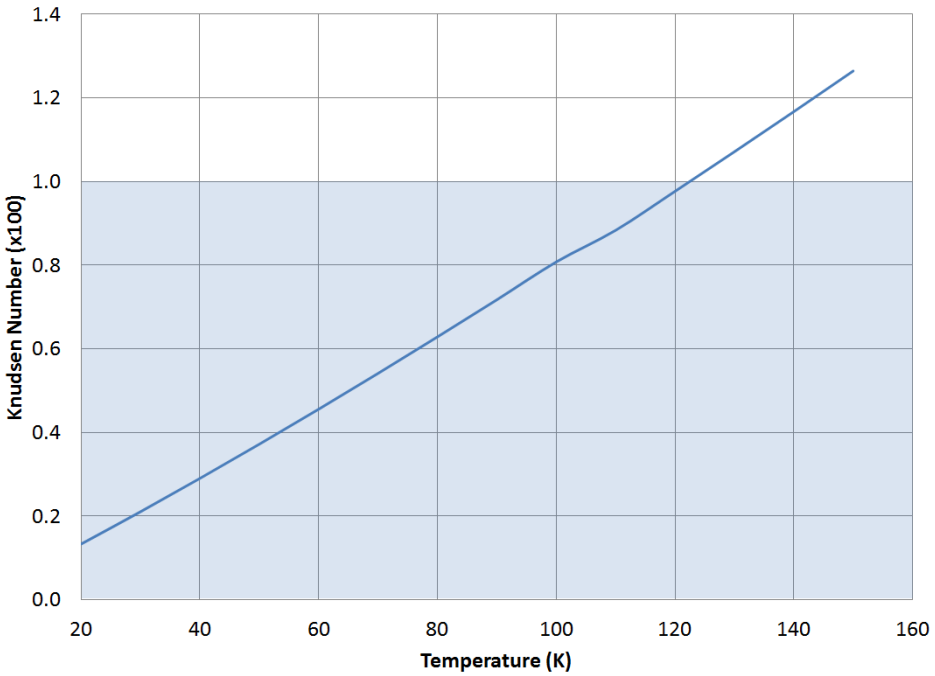

Figure 16. Knudsen Number in the XRCF Chamber During the First Cycle of Test 8 with Temperature.

4. Continuum Heat Transfer

The technique considered appropriate for a continuum gas heat transfer is to assume a single node within the chamber representing the rarified gas and to create couplings from that node to all surfaces in the chamber. The linear conductor is computed as the gas conductivity multiplied by surface area, then divided by an effective length. Dividing the gas into separate volumes within the chamber may have resulted in greater accuracy. For this effort, only one gas node was considered.

D. Gas Conduction Applied to XRCF Test 8

When these techniques were incorporated into the model of the XRCF cool down, both resulted in heat transfer rates that were far greater than was evident during the test as shown in Figure 17. The plot shows predicted temperatures for the center mirror (Segment A3) in the assembly along with the corresponding measured temperature from the test. Also shown in the figure is the predicted cool down rate of the mirror if no gas we introduced into the chamber.

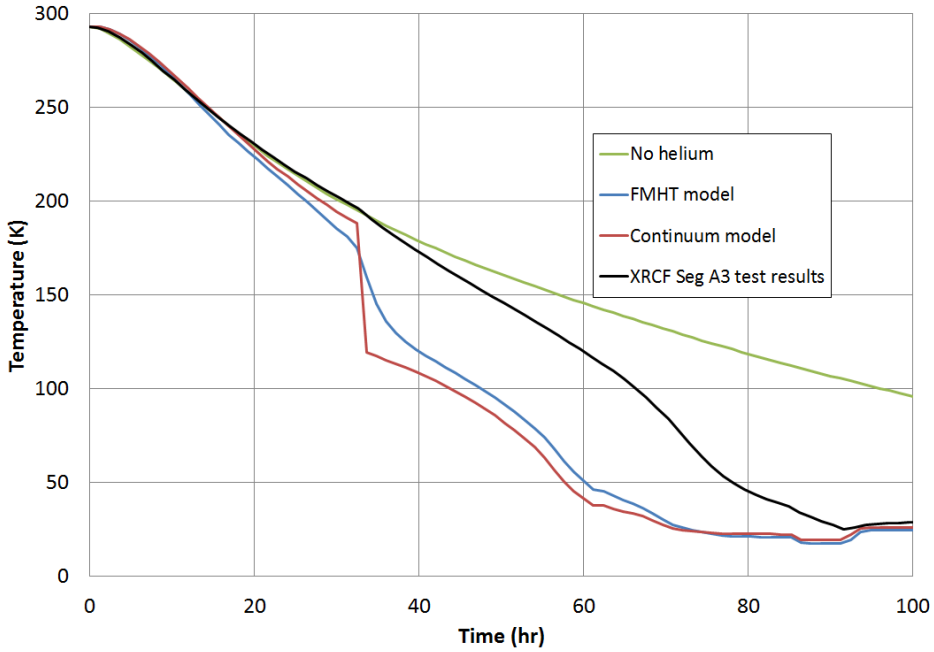

Figure 17. Comparison of Rarified Gas Heat Transfer Techniques for the XRCF Test 8 First Cycle Cool Down.

Applying correction factors with one of these techniques would have been a way to approach correlating the model results to test data, but uncertainties in a number of parameters need to be accommodated including the variable emissivity of the surface finishes as a function of temperature, accommodation coefficients and changes in their values with temperature and changes in the specific heat of materials with temperature. So an overall empirical correlation factor seemed more appropriate. The technique that was chosen involved using the FMC capability within SINDA/FLUINT with an empirical multiplication factor.

1. Empirical Correlation Results

Using the FMC capability within SINDA/FLUINT to correlate the model to test results involved assuming an accommodation coefficient of 1.0 for all surfaces, then applying a multiplier factor as a function of time. Since the gas pressure in the chamber for Test 8 was above that necessary for FMHT, applying a more accurate value for the accommodation coefficient isn't necessary. In fact, analytical results matched the test data quite well for Segment A3 when a constant value for the multiplier of 0.03 was applied for the first cool down cycle of Test 8 as shown in Figure 18. This figure also shows the pressure during the test with FMC multiplier. When helium was introduced into the chamber for this cool down, the pressure varied only slightly from 1.4 mTorr.

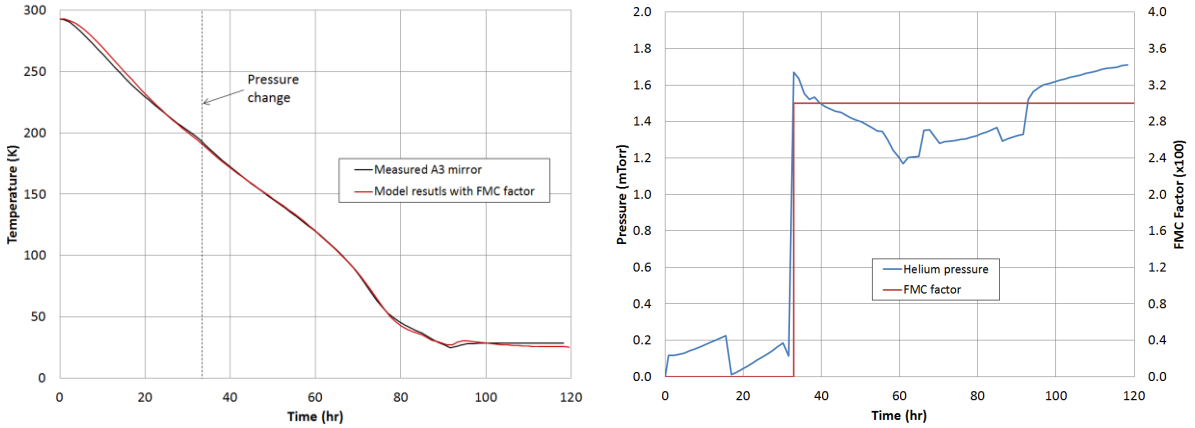

Figure 18. Correlation Results of Using FMC Multiplying Factor of 0.03 with Pressure about 1.4 mTorr for First Cool Down Cycle of Test 8.

During the second cooldown of Test 8, the helium pressure was initially about 1.0 mTorr but was then increased to about 1.8 mTorr after 28 hours. The test data clearly show an inflection in the data when the pressure was increased, indicting a clear dependence of heat transfer on pressure as show in Figure 17. Since the two pressures in the chamber during the second cool down bounded that in the first, these data implied a linear relationship between pressure and heat transfer. Figure 20 shows how well the correlation matched test data for Segment A3 for the two cool downs when the linear function of pressure was applied in the FMC multiplying factor.

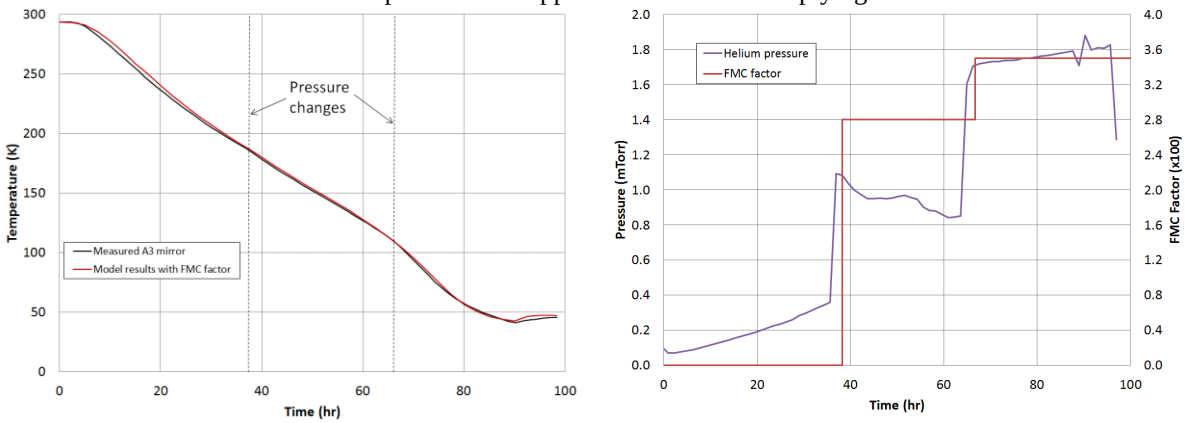

Figure 19. Correlation Results of Stepping FMC Multiplying Factor With Pressure for Second Cool Down Cycle of Test 8.

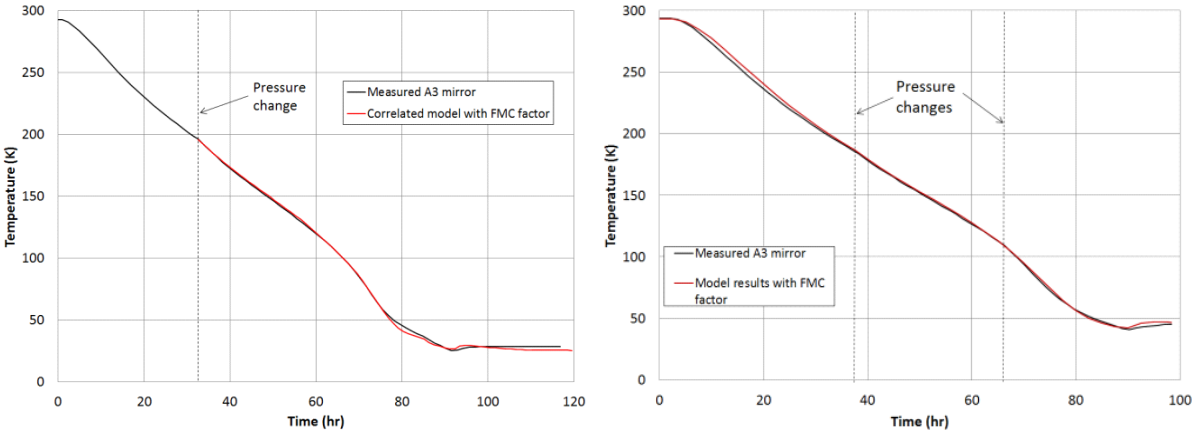

Figure 20. Correlation Results for Both Cycles (cycle 1 left, cycle 2 right) of Test 8 Using the Same Linear FMC Multiplying Factor.

E. Accounting for Variable Emissivity

As mentioned above, many of the thermal properties of the mirror assemblies change with temperature at colder temperatures. Simulating these effects is possible but requires considerably greater computing time than otherwise. For example, modeling variable emissivity for the back of the mirrors during the cool down of Test 8 cycle 1 requires 40 times the computational time than assuming a constant emissivity. To evaluate the effect of modeling with and without including variable emissivity, the analytically-determined heat transferred from Segment A3 to the chamber wall during the cool down was compared using constant emissivites and a variable emissivity based on Thomson's recommendation. This analysis is not intended to pertain to the correlation directly, only to estimate the potential error induced into predicted results by reducing computation time. Figure 21 shows the total heat transfer from Segment A3 mirror during the first cool down of Test 8. Also shown are the components of the total due to radiation and conduction. The conduction component is essentially all due to the correlated gas heat transfer due to the small thermal coupling between the mirror and whiffles and the small temperature difference between them. When helium is introduced, the radiative component is still far greater than that due to conduction; at the same time, the emissivity has only decreased by 7.5%.

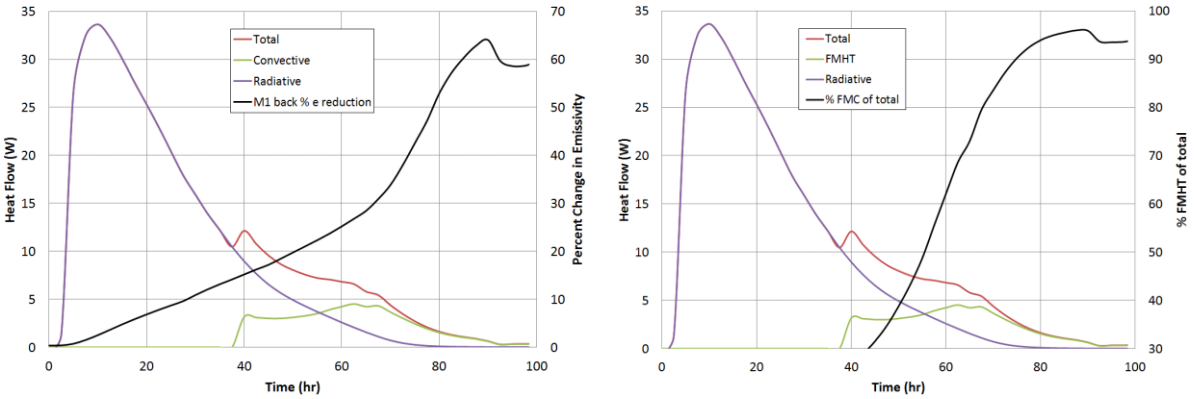

Figure 21. Calculated Heat Transfer from Segment A3 Mirror to Shroud with Percent Reduction in Mirror Back Emissivity on Left and Percent of Gas Heat Transfer to Total on Right.

At 60 hours, however, the gas heat transfer is 60% of the total and the emissivity has decreased 25%, so the total error would be about 10%. To give an indication of how this would apply to a cool down analysis, Figure 22 shows a comparison of analysis results using constant and variable emissivities for the back of the mirrors in the second cool down cycle of Test 8. A low constant emissivity of 0.25 relative to the average shows some discrepancy with the variable emissivity case, but using an average value of 0.4 or even the room-temperature effective emissivity of 0.48 matches the variable emissivity case well.

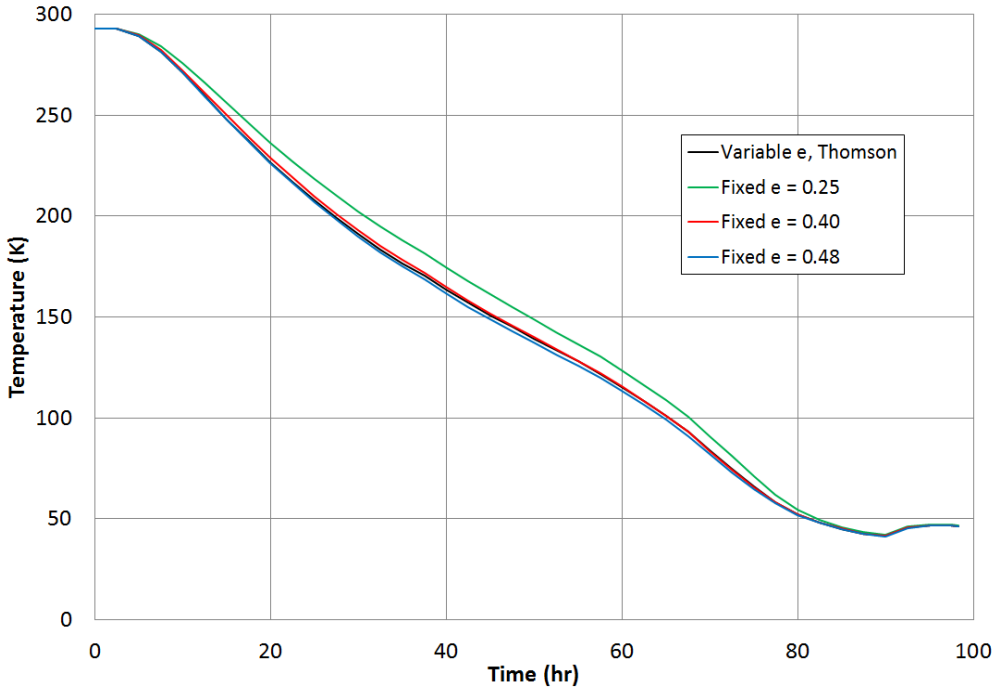

Figure 22. Parametric Analysis of Segment A3 Mirror Cool Down Using Constant and Temperature-dependent Emissivity for the Back of the Mirror.

One additional means of reducing the computation time required to simulate a cool down transient is to reduce the number of rays used in the ray tracing algorithm needed to determine radiative heat transfer between surfaces. The issue with this approach is a potential loss in accuracy. To evaluate any potential loss in accuracy, the cooldown simulations shown in Figure 22 were run with 50000 rays per node as compared to 5000 rays per node used to produce the curves shown in the figure. The maximum difference in temperature between the two methods at any time during the cool down for any of the cases was 0.3 K. Thus, at least for this analysis, 5000 rays per node provide sufficient accuracy.

F. Accounting for All Mirrors

Correlating with the FMC multiplying factor seems to work well as shown in Figure 20, but the only temperature shown is for the center of Segment A3 mirror. When we plot the rest of the mirrors from the same analysis result, we see that the others don't correlate as well (see Figure 23). It seems the other mirrors cool faster than the center mirror, which implies that there may be an additional heat transfer factor associated with the proximity of the mirrors to the chamber shroud. This also implies greater heat transfer between elements that are closer together. An option in Thermal Desktop® provides the distances between surfaces that could be used to input a second order heat transfer term to correct for this effect. The authors are currently working with the software vendor to include a factor based on relative distance between surfaces that can be included in the FMC calculations.

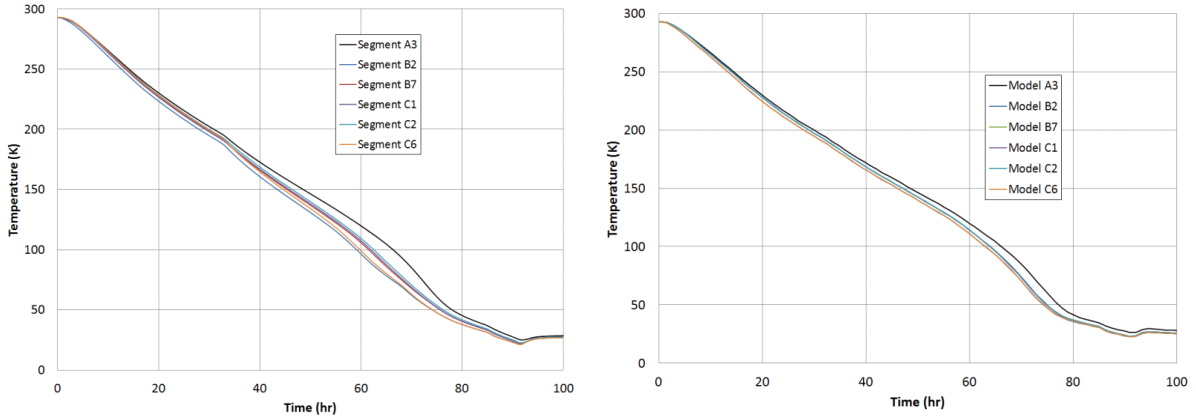

Figure 23. Measured (left) and Correlated (right) Temperatures of all Mirrors During the First Cycle of Test 8.

Another option for correlating PMSA cooling after helium has been introduced is to consider the constant emissivity of the back of the mirrors used to achieve the data shown in Figure 20 and Figure 23. While we've shown above that the effects of variable emissivity are minimal below about 100 K where they are changing the most, the specific value used for emissivity between 100 and 200 K is significant. The results shown in Figure 20 and Figure 23 were achieved when a constant emissivity of 0.2 was used for the backs of the mirrors. If we assume a constant mirror back emissivity of 0.3, we obtain the cool down profiles shown in Figure 24. The black lines in the figures show actual measured temperatures during the test and the red lines, simulation results. While the simulation of the center mirror (Segment A3) is more accurate using a mirror back emissivity of 0.2, correlation is better for all of the mirrors assuming a constant emissivity of 0.3. There still is an indication of improvement with consideration for proximity to the shroud, as Segments B2 and C6 are closest to the colder shroud base (see Figure 10), but the correlation is better all around.

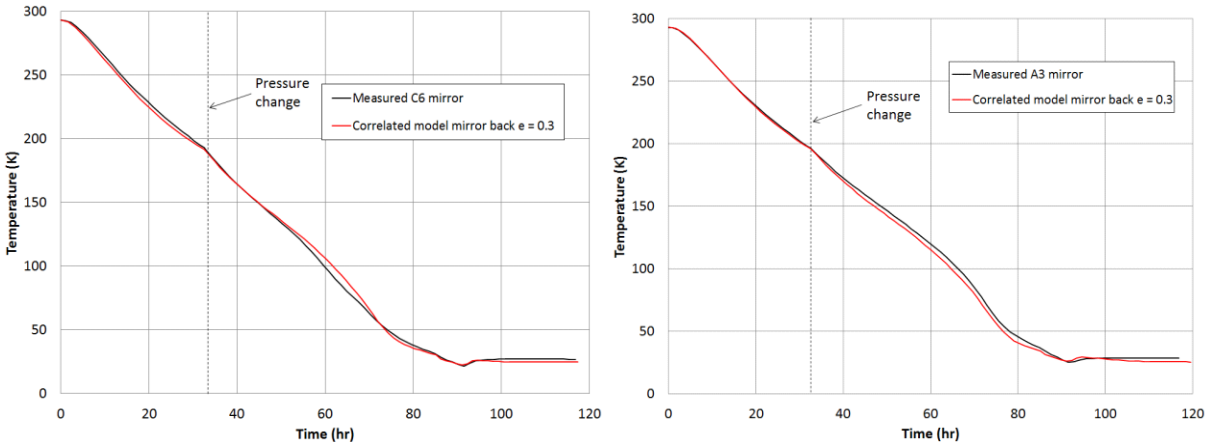

Figure 24. Measured and Correlated Mirror Temperatures During First Test 8 Cycle With Constant Mirror Back Emissivity of 0.3.

G. Accounting for All Components

While the correlation of mirrors is good with this technique, temperature results for other PMSA components are less compelling. Figure 25 shows test results for Segment A3 PMSA components along with model results for the same simulation as Figure 23. The correlation works relatively well above about 75 K and a little worse for the delta frame, but all show significant difference below that temperature. It seems the correlation technique presented above under predicts gas heat transfer at the colder temperatures. Including a proximity term may improve these results.

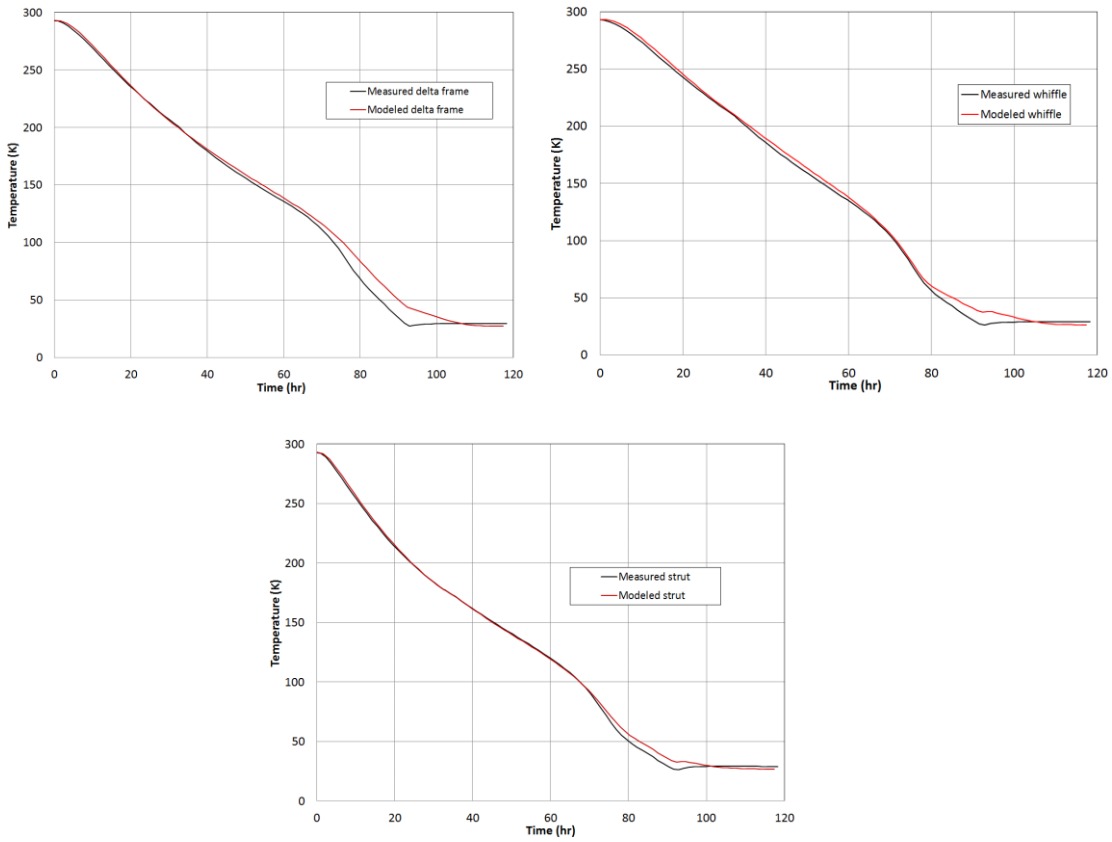

Figure 25. Measured and Correlated Temperatures for Segment A3 Delta Frame, Whiffle and Strut.

H. PMSA Temperature Constraints

The primary reason for correlating XRCF test data is to gain confidence in predicting PMSA temperatures in future testing, so that we can be assured that differential temperature constraints between components will not be exceeded. The three primary constraints are defined for the difference between the mirror and delta frame, that between the mirror and whiffle and that between the strut and its mounting point on the mirror. In Figure 26 the solid lines are the constraints defined by PMSA structural engineers and the dashed lines show the temperature differences that occurred during the Test 8. This chart shows that differences in temperature during the XRCF testing were well within required limits. One interesting point to note is that the differences in temperature that come closest to the constraints occurred for all three components before helium was introduced in the chamber.

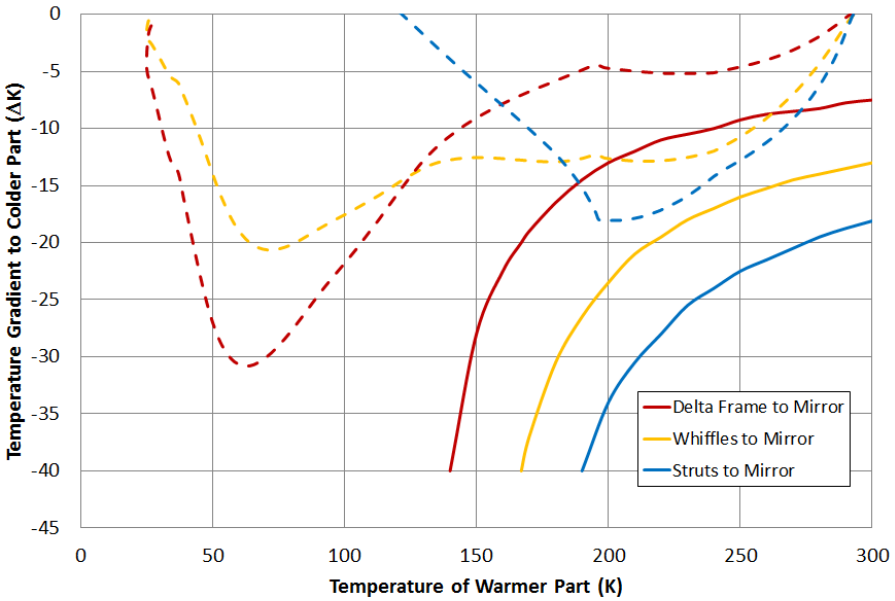

Figure 26. A3 PMSA Differential Temperature Constraints and Corresponding Differences During XRCF Test 8 Cycle 1 Cool Down.

Figure 27 shows the same temperature differences measured from the Test 8 and the corresponding analysis predictions. The greatest differential temperature errors in the model results occur when the biggest temperature discrepancies in the analysis are present as shown in Figure 25. These errors are largest at the colder temperatures. The constraints are less severe at the colder temperatures and future improvements in the correlation should, at a minimum, emphasize the correlation at warmer temperatures.

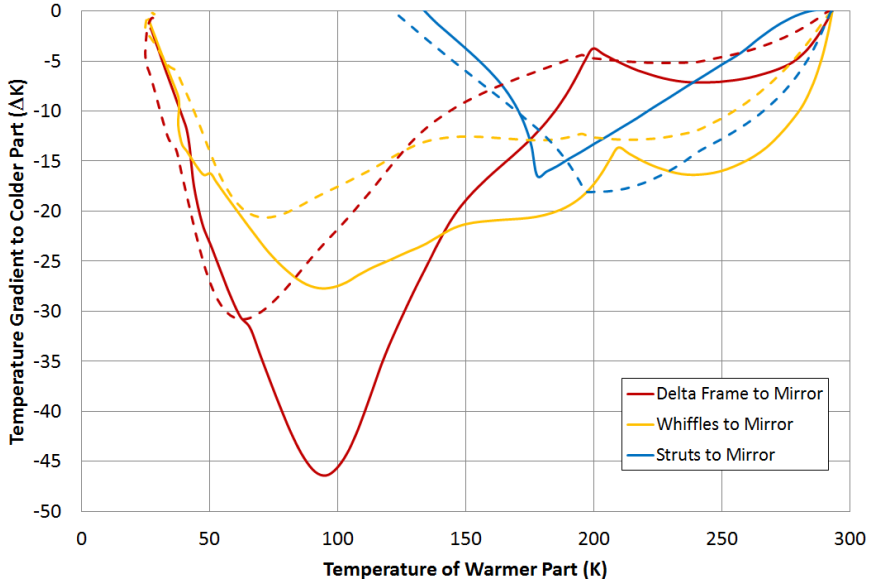

Figure 27. Comparison of PMSA component temperature differences between XRCF Test 8 and analysis results for Segment A3.

I. Gradient within Mirrors

With the added fidelity in the simulation of the mirrors from 1 to 32 nodes, it is possible to evaluate the capability of the model to predict mirror gradients. Figure 28 shows the predicted gradients in the mirror during the first test cool down, and clearly displays the effect of proximity cooling to the shroud. The platen on which the

mirror assembly was mounted cooled faster in the test than the rest of the shroud, and the effect is seen in the lower portions of Segments B2 and C6. The current model over predicts gradients in the mirror after helium is in the chamber showing a maximum difference between the edge and center of about 2.0 K compared to test results which showed a maximum difference of about 1.3K.

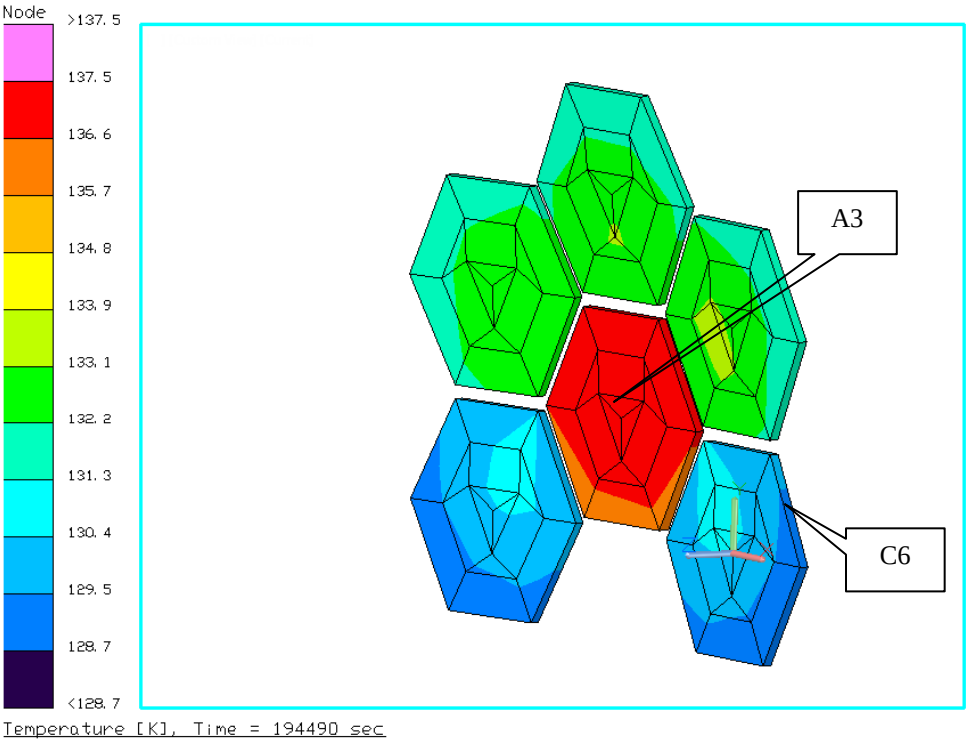

Figure 28. Temperatures Differences Within the Segment Mirrors During Test 8 of XRCF Testing.

VI. Conclusion

The JWST optical element thermal models are evolving to more accurately predict temperatures during cooldown and warmup at ground tests. This evolution includes improvements in temperature predictions for test environments that use rarified gas to accelerate transition. Existing test data from subsystem level testing is being used to correlate the models. Limitation and constraints for the PMSA's have been presented and discussed. Progressions of the model development and potential improvements on the current correlation have been discussed.

Acknowledgments

The authors would like to acknowledge the test and thermal engineers across the program past and present who have contributed to the current body of knowledge which aids in this effort. Also the authors would like to acknowledge the JWST Thermal Working Group (TWG) and the Thermal Test Working Group (TTWG) and the collaborative and positive engineering environments that they maintain.

References

[1]Park, S., Ousley, W., Cohen, L., Parrish, K., Burt, W., "James Webb Space Telescope Pathfinder First Cryogenic Test Thermal Analysis", 42nd International Conference on Environmental Systems, AIAA, Washington, DC, 2012

[2]Thomson, S., "Calculation of Primary Mirror Rear Surface Effective Emissivity," NASA TR-11-008, 2011.